Supplementary Information

Supplementary materials and methods

Flow cytometric analysis

Cells obtained from different organs were labeled with monoclonal antibodies (mAbs) and analyzed with FACSAria or FACSCanto II (BD Biosciences). For intracellular cytokine staining, mouse splenocytes were stimulated with 25 ng/ml PMA (Sigma), 10 mg/ml ionomycin (Sigma), and 1 mg/ml anti-CD28 Ab (CD28.2, BD Biosciences) in RPMI-1640 supplemented with 10% FBS at 37℃. After 1 hour incubation, 10 mg/ml brefeldin A (Sigma) was added, and further incubated at 37℃ for 3 hours. After staining surface antigens, cells were fixed and permeabilized using BD Cytofix/Cytoperm™ Fixation/Permeabilization Kit (BD Biosciences), and stained with anti-IFN-γ and anti-IL-17A antibodies.

Antibodies

Cells labeled with the following monoclonal antibodies were analyzed and/or sorted using FACSAria and FACSCanto-II (BD Biosciences): anti-hCD3 BV421™ (clone UCHT1, RRID:AB_11152082), -hCD3 Allophycocyanin (APC) (HIT3a, RRID:AB_398592), -hCD4 PE-cy7 (SK3, RRID:AB_400379), -hCD8 APC-cy7 (SK1, RRID:AB_400383), -hCD19 PE-cy7 (SJ25C1, RRID:AB_400217), -hCD25 BV421™ (M-A251, RRID:AB_11153864), -hCD33 PE (WM53, RRID:AB_395843), -hCD34 PE-cy7 (8G12, RRID:AB_400381), -hCD38 APC (HB7, RRID:AB_400512), -hCD45 FITC, APC, and BV421™ (HI30RRID:AB_395874, AB_398600, AB_2744402), -hCD45 APC-cy7 (2D1, RRID:AB_1645735), -hCD45RA FITC (HI100, RRID:AB_395879), -hCD56 FITC (NCAM16.2, RRID:AB_400025), -hCD183 PE (1C6, RRID:AB_396596), -hCD196 PE (11A9, RRID:AB_394247), -hIFN-γ FITC and PE (B27, RRID:AB_395517, AB_559327), -hTCRγδ FITC (11F2, RRID:AB_400358), -mCD45 APC-cy7 and BV510™ (30-F11, RRID:AB_396774, AB_563891), -CD324 eFluor660 (DECMA-1, RRID:AB_11043137) (all from BD), -hFoxp3 APC (PCH101, RRID:AB_1603281), -hIL-17A FITC (eBio64DEC17, RRID:AB_10805390) (all from eBioscience), -hIL-17A PE (BL168, RRID:AB_961394) (from Bio Legend), -hTCRαβ PE (IP26A) (from BECKMAN COULTER).

Histological analysis

Tissues were fixed with 4% paraformaldehyde and embedded in paraffin. Sections were stained with hematoxylin and eosin. For immuno-histochemical staining, deparaffinized sections were treated with heat-induced antigen retrieval solution (Retrievagen A solution (pH 6.0, BD Pharmingen™) or Retrievagen B solution (pH 9.5, BD Pharmingen™)). After blocking endogenous peroxidase activity using H2O2 and non-specific binding of antibodies with 2.5% horse serum, slides were incubated with the primary following antibodies: mouse anti-human CD45 (2B11+PD7/26, Dako, RRID:AB_2661839), mouse anti-human CD3 (PS1, Abcam, RRID:AB_305686), mouse anti-human CD4 (BC/1F6, Abcam, RRID:AB_306570), mouse anti-human CD8 (C8/144B, Dako, RRID:AB_2075537), mouse anti human-CD68 (KP1, Abcam, RRID:AB_307338), mouse anti-human-cytokeratin13 (AE8, Abcam, RRID:AB_302267), rabbit anti-cytokeratin15 (EPR1614Y, Abcam, RRID:AB_869863), rabbit anti-cytokeratin17 (EP1623, Abcam, RRID:AB_10889888), and rabbit anti-cytokeratin19 (EP1580Y, Abcam , RRID:AB_765002). Horseradish peroxidase-conjugated anti-mouse / rabbit antibody (ImmPRESS MP-7500, VECTOR) were used as secondary antibodies. 3,3'-diaminobenzidine was used as the chromogen (SK-4100, VECTOR) and hematoxylin was used as a counterstain. Light microscopy was performed using an Axiovert 200 (Carl Zeiss).

qPCR Analysis

Total RNA was extracted from brain, liver, lung, spleen, salivary gland and skin in a hIL-6 Tg NSG recipient using Trizol reagent (ThermoFisher Scientific). A Custom TaqMan Array of human cytokine/chemokine was designed as described in

Table S4 (ThermoFisher Scientific). The expression level of human cytokine /chemokine was estimated by ViiA7 Real-Time PCR System (ThermoFisher Scientific).

Fig. S1

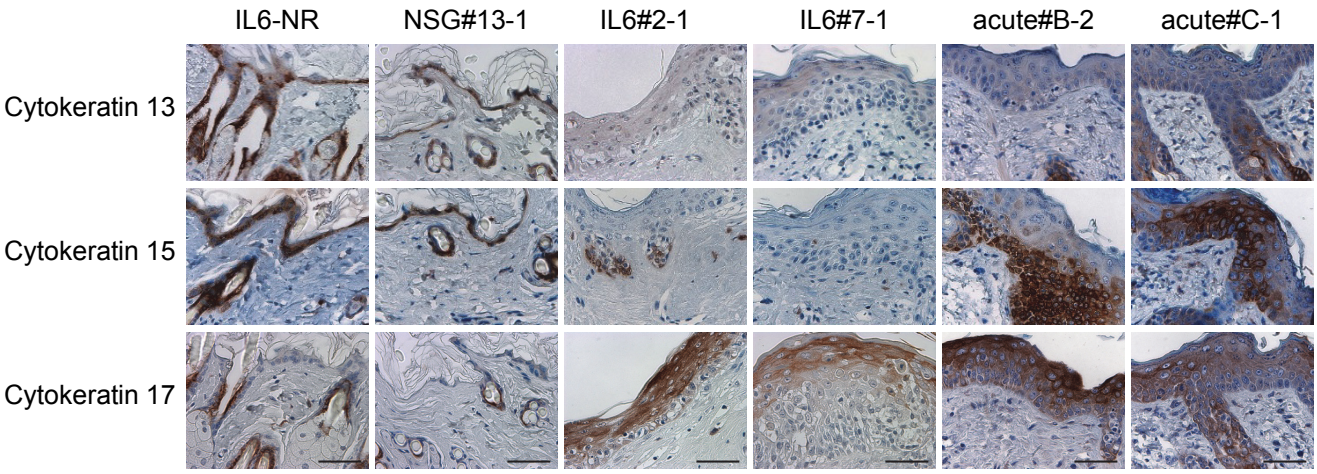

Fig. S1. Altered expression of skin cytoskeletal filaments.
IHC staining of cytokeratin13 (upper panels) , cytokeratin15 (middle panels), and cytokeratin17 (lower panels) in skin sections of hIL-6 Tg NSG mouse without transplantation (IL6-NR), hIL-6 non-Tg NSG recipient (NSG#13-1), hIL-6 Tg NSG recipients (IL6#2-1, IL6#6-1), and acute GVHD humanized mice (acute#B-2, acute#C-1). Acute GVHD mice are characterized by overexpression of cytokeratin15 and cytokeratin17 and by decreased expression of cytokeratin13, while hIL-6 Tg NSG recipients are characterized by overexpression of cytokeratin17 and by decreased expression of cytokeratin13 and cytokeratin15 in epidermis. Bars: 50μm.

Fig. S2

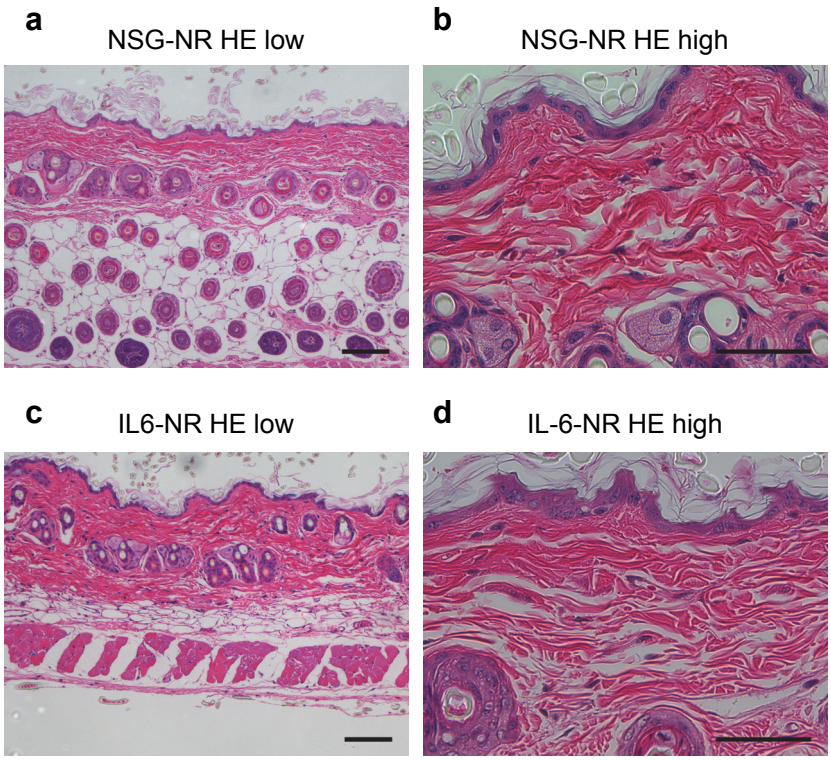

Fig. S2. Histological analysis of control mice.
(a, b) H&E staining sections of hIL-6 non-Tg NSG mouse and (c, d) hIL-6 Tg NSG mouse without transplantation. These control mice show no abnormal findings in epidermis and dermis. Bars: (a, c) 50μm; (b, d) 100μm.

Fig. S3

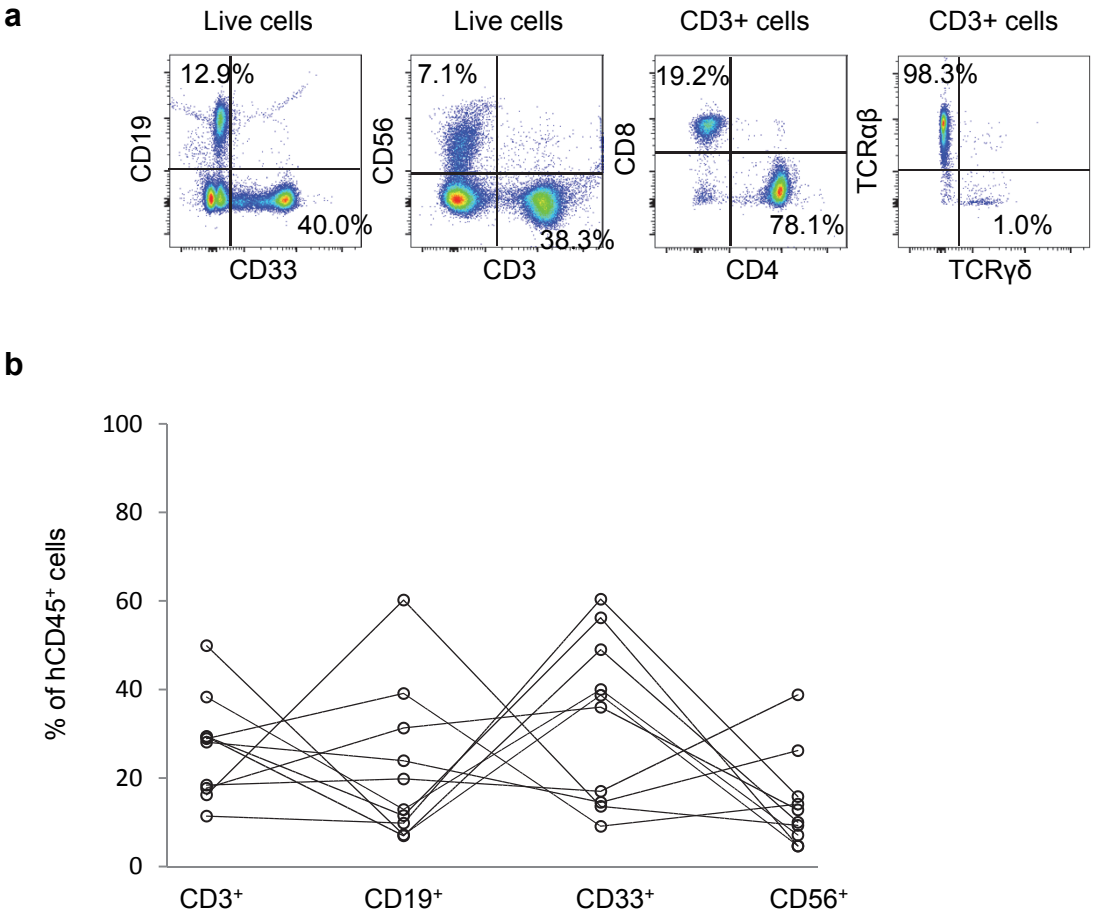

Fig S3. Immune cell subsets of human CB CD34$^-$ fraction.
(a) Representative flow cytometry plots of human CB CD34$^-$ fraction. In addition to CD4$^+$ and CD8$^+$ T cells, CD19$^+$ B cells, CD33$^+$ myeloid cells, and CD56$^+$ NK cells were detected. (b) Summary of human immune cell subset in CD34-negative faction of human CB (n=10).

Fig. S4

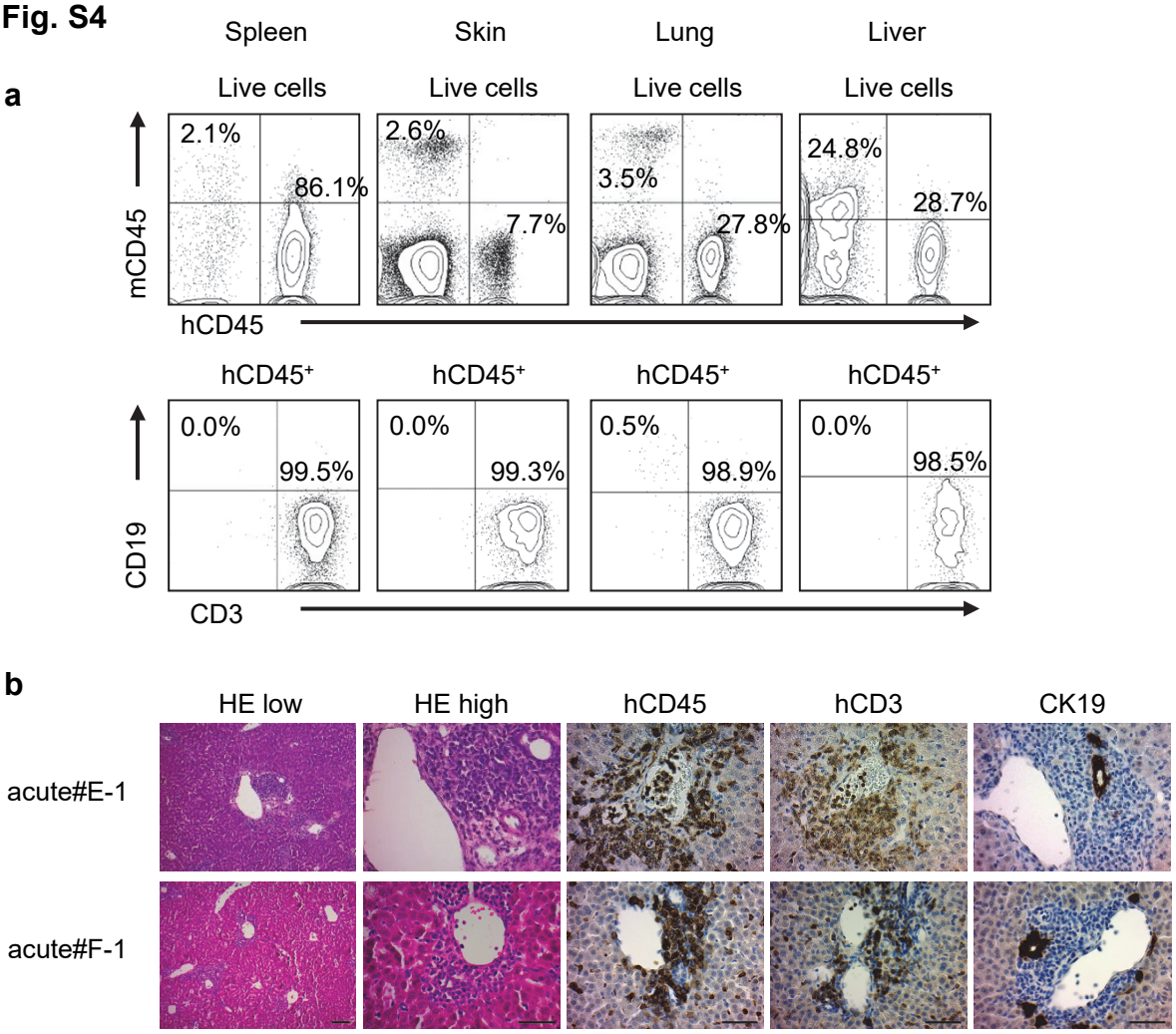

Fig S4. Modeling acute GVHD in NSG mice.
(a) Representative flow cytometry plots of acute GVHD NSG humanized mouse (mouse ID: acute#B-3). (b) Histological analyses of the liver of acute GVHD mice (acute#E-1, acute#F-1). T cell infiltration around cytokeratin19 positive bile ducts is characteristic. Few $CD68^{+}$ macrophages are detected in the liver. Reduction of bile ducts or portal fibrosis is not observed. Bars: (far left) 100μm; (the others) 50μm.

Fig. S5

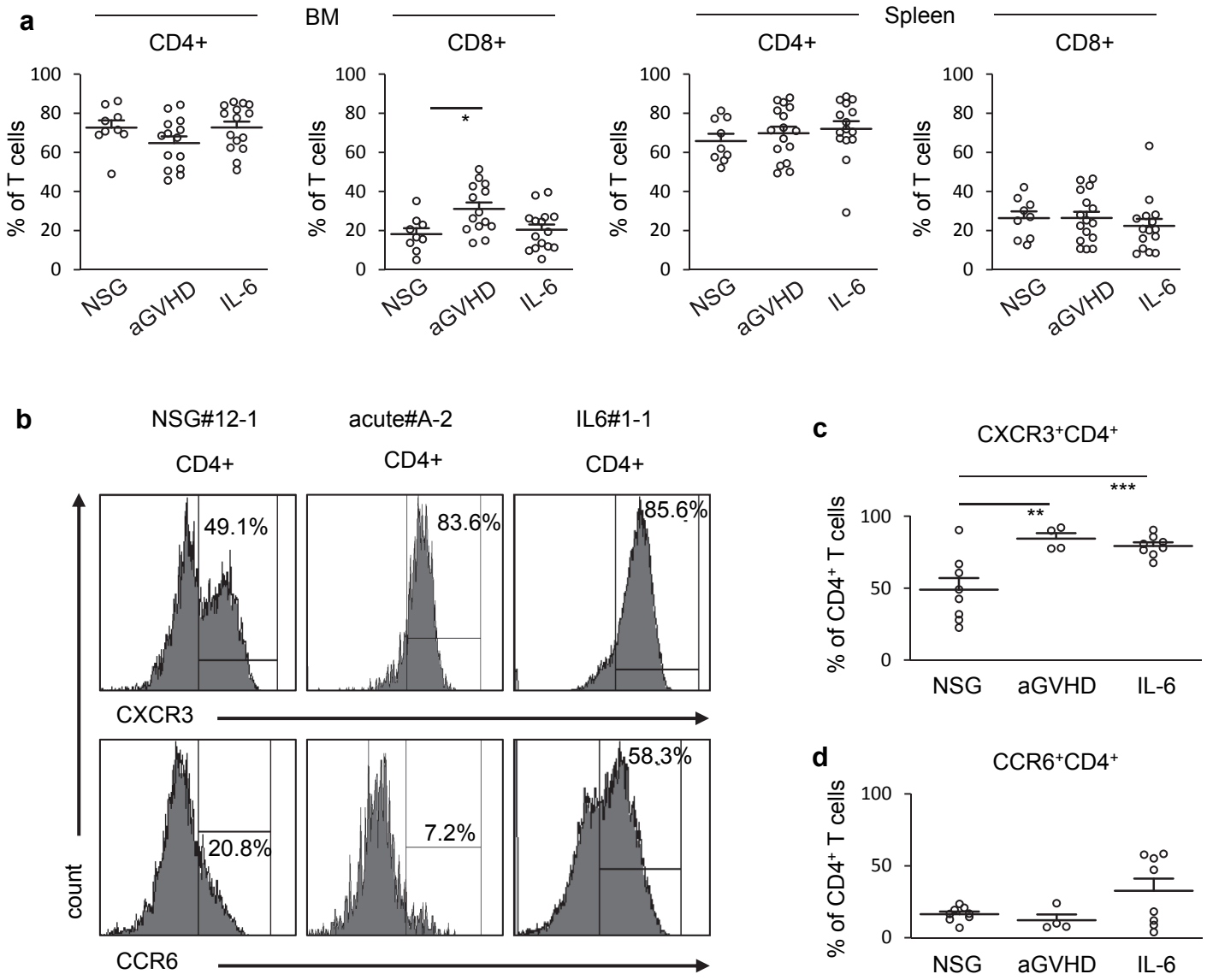

Fig. S5. Comparison of T cell biology among humanized mouse models.
(a) Frequencies of CD4+ and CD8+ cells in human T cells in the BM and spleen of hIL-6 non-Tg NSG recipients (NSG, n=9), acute GVHD humanized mice (BM-aGVHD, n=14, spleen-aGVHD, n=16), and hIL-6 Tg NSG recipients (IL-6, n=15). (b) Representative flow cytometry plots of human CD4$^+$ spleen T cells of humanized mouse stained with CXCR3 (upper panels) and CCR6 (lower panels). (c, d) Summary of chemokine receptor analyses of mouse splenic CD4$^+$ T cells. hIL-6 non-Tg NSG recipients (NSG; n=8), acute GVHD model mice (aGVHD; n=4), and hIL-6 Tg NSG recipients (IL-6; n=8) are analyzed for (c) CXCR3 and (d) CCR6. *P = 0.01, **P = 0.01, ***P = 0.003 by 1-way ANOVA with Bonferroni post-test. Error bars represent mean ± SEM.

Fig. S6

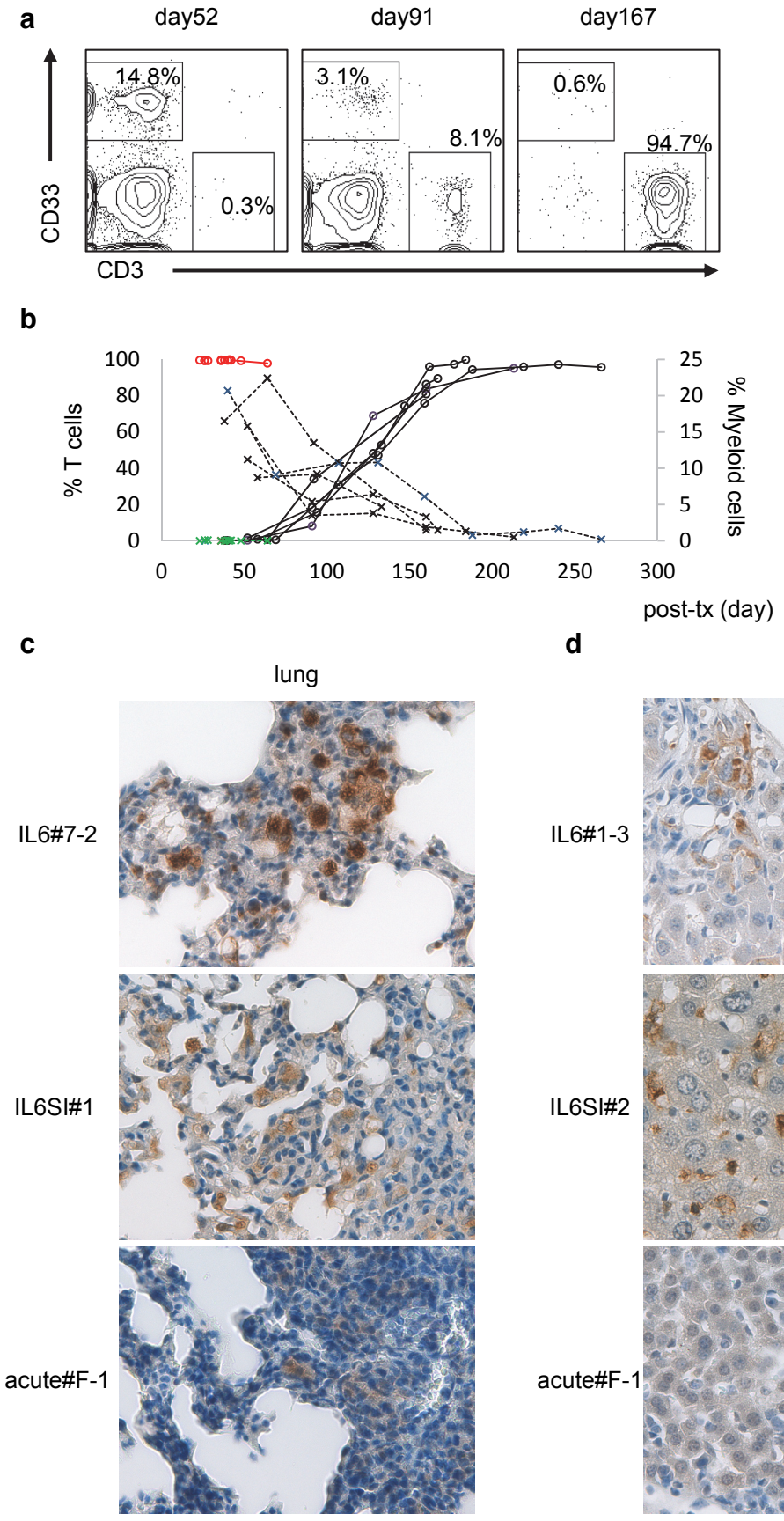

Fig. S6. Evaluation of myeloid cells in GVHD humanized mouse models.
(a) Representative flow cytometry plots of PB of a hIL-6 Tg NSG recipient (IL6#3-1). (b) Frequency of T cells (circle mark) and myeloid cells (cross mark) in PB of hIL-6 Tg NSG recipients (black; n=5) and that of acute GVHD mice (red and green; n=11). (c, d) Comparison of infiltrated macrophages between acute and chronic GVHD humanized mouse models. CD68-IHC staining section of lung (c) and liver (d) of hIL-6 Tg NSG humanized mice (top and middle panels) and acute GVHD humanized mice (lower panels). Bars: 50μm.

Fig. S7

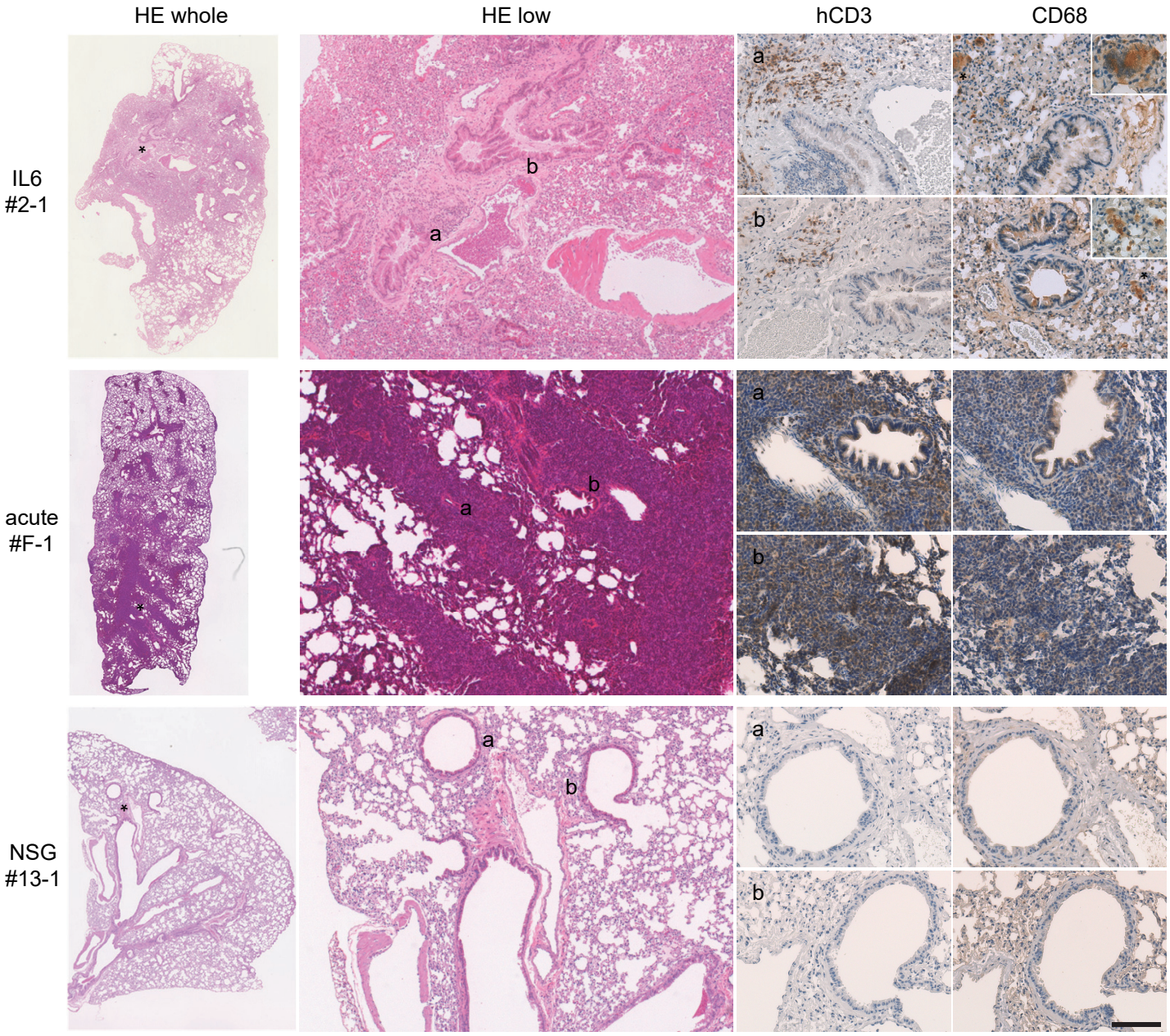

Fig. S7. Fibrosis of peri-bronchiolar areas and infiltration of T cells and macrophages in the lung of hIL-6 Tg NSG humanized mice.
Lung sections of a hIL-6 Tg NSG recipient (IL6#2-1, top panels), an acute GVHD humanized mouse (acute#F-1, middle panels) and a non-Tg NSG recipient (NSG#12-1, bottom panels). HE-stained whole lobes (the left end panels) and the peri-bronchiolar areas indicated by asterisks (the second left panels) are shown. Immunohistochemical staining for $CD3^+$ human T lymphocytes (the second left panels) and $CD68^+$ macrophages (the right end panels) are shown. In the IL-6 Tg NSG recipient and in the acute GVHD humanized mouse, a number of human T cells were present. In the IL-6 Tg NSG recipient, $CD68^+$ macrophages were also found in the indicated areas (a and b in the second left panels). High magnification of the infiltrated macrophages are shown in the right upper corner. Bars: 100μl.

Fig. S8

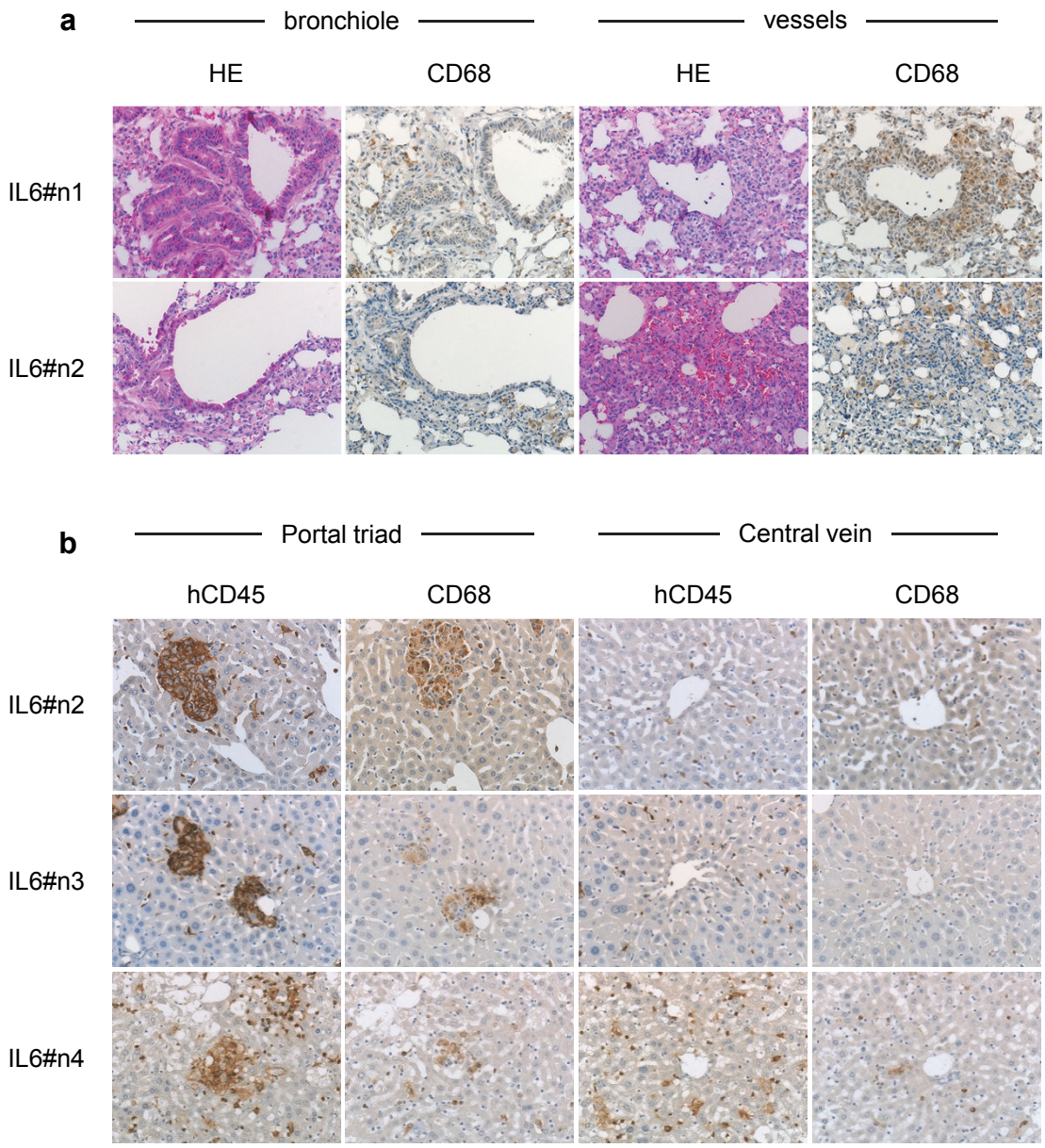

Fig. S8. Lung and Liver histology in IL-6 Tg NSG humanized mice without macroscopic skin lesions.
(a) Lung sections of hIL-6 Tg NSG humanized mice without macroscopic skin lesions (n=2; IL6#n1, IL6#n2). HE and CD68 stained sections of peri-bronchiole area (left panels) and peri-vascular area (right panels) are shown.
(b) Liver sections of hIL-6 Tg NSG humanized mice without macroscopic skin lesions (n=3; IL6#n2, IL6#n3, IL6#n4). hCD45 and CD68 stained sections of portal triads (left panels) and peri-central vein area (right panels) are shown..

Fig. S9

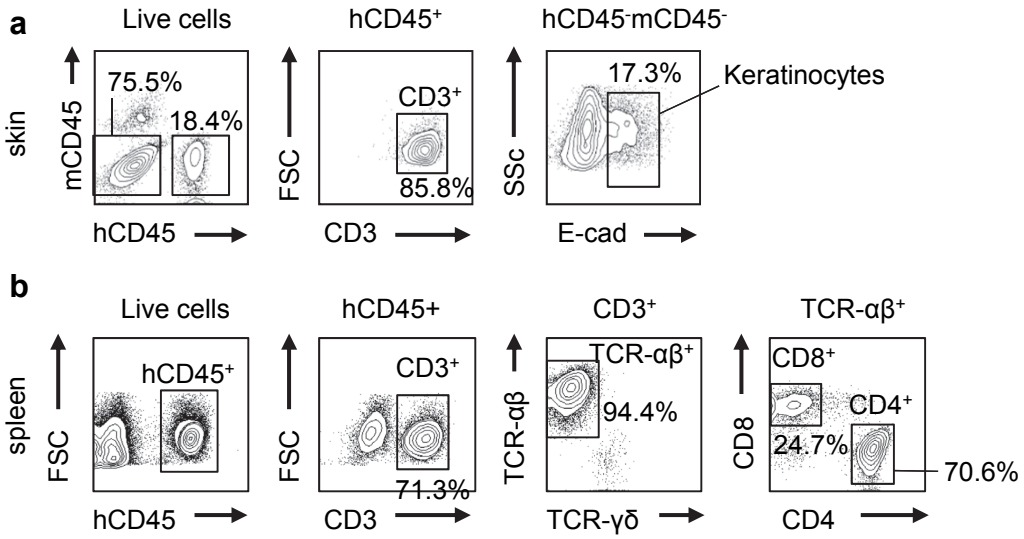

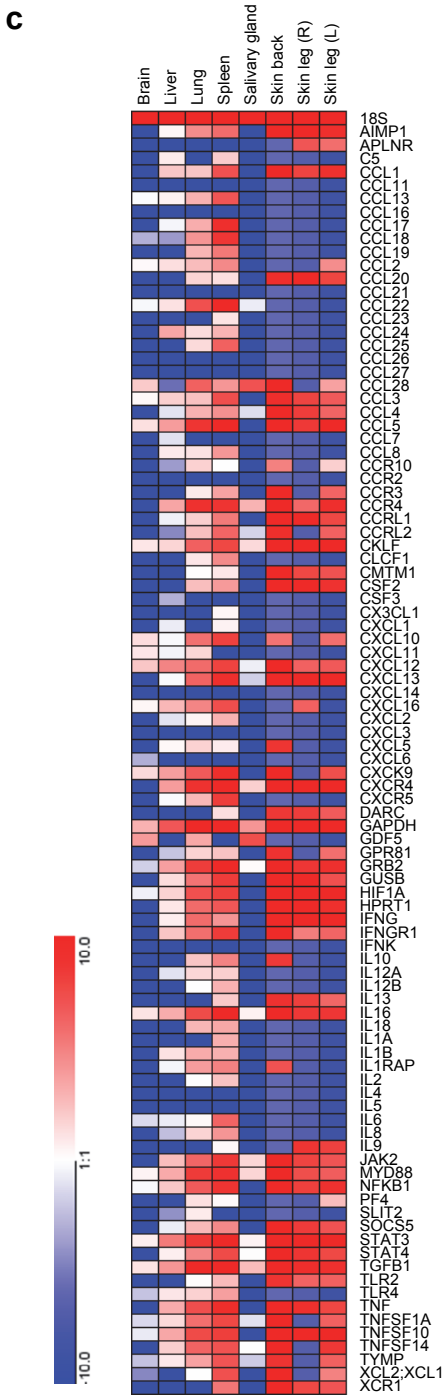

Fig. S9. Transcriptomic analyses of chronic GVHD model mice. (a, b) Sorting strategy of (a) mouse skin cells, and (b) splenocytes for RNA sequencing (IL6#5-1). (c) Comparison of gene expression signature among different organs of a chronic GVHD mouse. Global transcriptional profiles among different organs including brain, salivary gland, liver, lung, spleen, and skin (back, right leg and left leg) from single hIL-6 Tg NSG recipient.